Misleading residues on lithics from Star Carr: identification with Raman microspectroscopy

Shannon Croft[a,*], Konstantinos Chatzipanagis[b], Roland Kröger[b], Nicky Milner[a]

[a,*] Department of Archaeology, King's Manor, University of York, York, YO1 7EP, UK
[b] Department of Physics, University of York, Heslington, York, YO10 5DD, UK

[*]Corresponding author. E-mail address: shannon.croft@york.ac.uk (S. Croft)

ABSTRACT

Ancient trace residues left on stone artefacts by people represent a source of potentially fruitful data about diet, technology, and behaviour, but their investigation is not problem-free. Rather, correct identification of degraded residues and determination of their natural or anthropogenic origin remains at the heart of current methodological development in lithic residue analysis. It is increasingly becoming clear that reflected visible light microscopy (VLM) is insufficient to make secure identifications of ambiguous residues. Confocal Raman microspectroscopy (micro-Raman) is a non-destructive technique that can identify the specific molecular nature of microscopic residues with high spatial resolution. Here, the identification of artefact residues as anthropogenic by visual inspection alone was found to be incorrect in all cases tested. Micro-Raman provided the key source of information to unambiguously determine the chemical nature of residues and hence their origin.

Keywords:
Non-anthropogenic residues; iron oxide; gypsum; quartz; reflected visible light microscopy (VLM); confocal Raman microspectroscopy (micro-Raman)

1. Introduction

The ideal goal of residue analysis on stone tools is to arrive at a detailed account of the use of objects by humans in the past, and/or reconstruct technological choices made during manufacturing activities. This goal is complicated by three major issues in residue analysis, as outlined by outlined by Grace (1996), Haslam (2006a), and Langejans (2009):

1) Residues might be due to contamination rather than human use. The presence of contaminants on artefacts originating from the burial environment or post-excavation sources are a significant concern.

2) Researchers are still unable to describe the mechanisms of residue preservation. The chemical mechanisms that degrade residues as related to specific burial environments are not well-understood. This means analysts may be unaware of processes that are affecting the lithic assemblage under study.

3) Residues on a tool could be a palimpsest of events and it is impossible to distinguish these different events. Residues of the same or different type are not necessarily related in time, and the tasks to which artefacts are put can vary throughout the course of use.

These three methodological issues are all important considerations in the development of lithic residue analysis. Nevertheless, an issue regarding residue interpretation can be added to this list of challenges:

4) Residues may be identified incorrectly due to insufficient information.

Specific and accurate identification to differentiate between anthropogenic and non-anthropogenic or 'contaminant' residues on stone tools remains a crucial issue, and has been highlighted recently by Monnier et al. (2012), Croft et al. (2016), and Pedergnana and Blasco (2016). New emerging techniques are providing more objective identifications that are less susceptible to interpretative mistakes. Among them are Fourier transform infrared spectroscopy coupled to a microscope (FTIRM) (Monnier et al., 2017a, 2017b), gas chromatography-mass spectrometry (GC-MS) (Bleicher et al., 2015; Helwig et al., 2014; Luong et al., 2017), and Raman microspectroscopy (micro-Raman) (Bordes et al., 2017; Monnier et al., 2013). This increase in the use of verifiable techniques in residue analysis is perhaps not a surprise. Molecular level analysis is widely regarded as a vital tool responsible for expanding the knowledge base in archaeological studies.

Here, we present three residue types encountered in a sample of lithics from Star Carr where micro-Raman demonstrated that the proposed residue identities based on microscopic visual characteristics alone were incorrect. Other methods of investigation, including variable pressure scanning electron microscopy equipped with energy dispersive X-ray spectroscopy (VP-SEM-EDS), FTIRM, and GC-MS, were also used to try to discern the chemical identity of residues. However, micro-Raman provided the clearest and most specific results for the three residue types tested.

2. Site and samples

The lithic sample was excavated at the Early Mesolithic site of Star Carr, in the Vale of Pickering, UK (Fig. 1). The site is within wetland peat deposits and is famous for its preservation of organic artefacts. The first Mesolithic human activity at Star Carr is modelled with radiocarbon dates to start at *9385–9260 cal BC* (*95% probability*), and end at *8555–8380 cal BC* (*95% probability*) (Bayliss et al., in press Fig. 17.2).

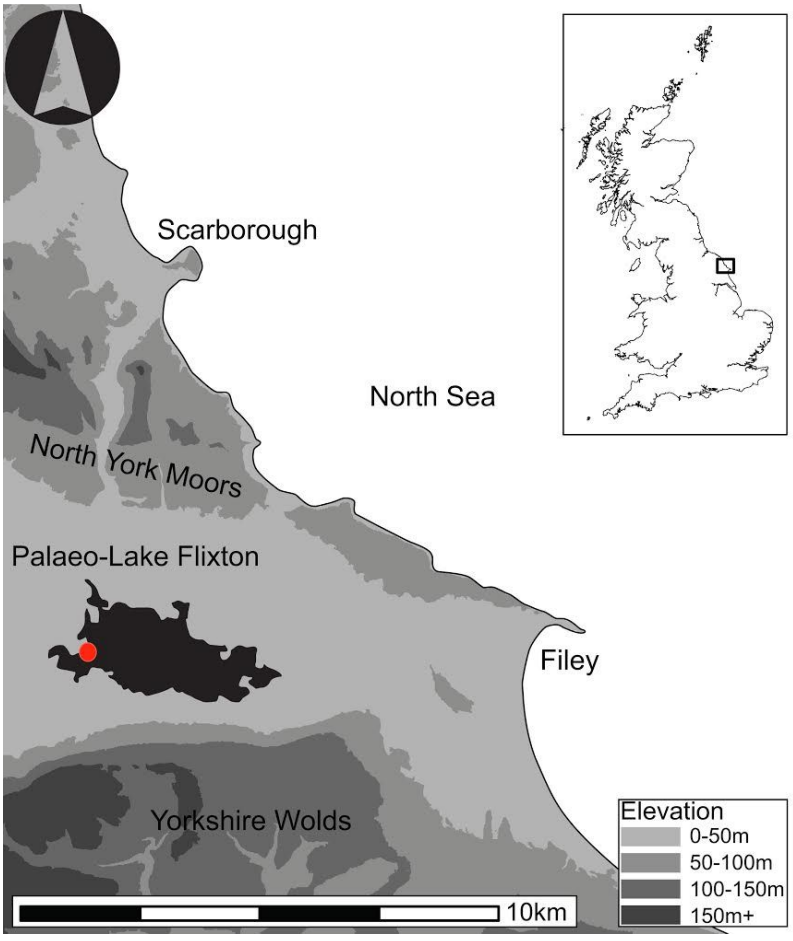

Fig. 1. Location of the site of Star Carr in North Yorkshire, UK. (Sourced from Milner et al. 2016, *Internet Archaeology* licenced under CC-BY 2.0)

A total of 614 stone tools and 614 sediment samples were excavated at Star Carr specifically for residue analysis. Of these, 138 stone tools were examined microscopically, followed by chemical characterisation of selected residues and sediment samples.

3. Method

3.1 Anti-contamination protocols and cleaning

Artefacts were handled with care to minimise contamination. No other types of analyses, such as lithic typo-technological analysis, morphometrics, or refitting took place prior to residue analysis, minimising the introduction of modern contaminants from handling or curation practices such as the addition of tape, ink, glue, or nail polish. On site at Star Carr, excavators collected each lithic for residue analysis by inserting a trowel into the soil just below the lithic and levered it directly into a polyethylene zip bag, without touching the lithic. A small sediment sample (~ 5 g) was taken below each lithic with a trowel and placed in a zip bag. Lithics and soil samples were stored in a fridge at 5°C to slow the decomposition of any potential archaeological residues by fungi, bacteria, microorganisms, and/or worms and insects. Each lithic was handled with gloves which were changed between samples to prevent cross-contamination. The non-powdered gloves (semperguard®) used were microscopically inspected – and negative – for starch.

After excavation, all stone tools had peat or clay-rich deposits adhering to their surfaces. A cleaning treatment was required to allow residues to be seen during microscopic examination. After testing several lithic cleaning methods, it was determined that the most suitable method was a wash with ultrapure water expelled from a squeeze bottle and gentle rubbing each lithic with a gloved hand. Following washing, each lithic was set to dry next to its associated bag on a tray lined with a new sheet of cling film, making sure no lithics or bags touched each other.

To provide a support on the microscope stage that minimised contamination and the loss of residues, the stage was prepared by placing a bed of Blu-Tack® on the stage and then overlaying a new layer of plastic paraffin film (Parafilm M®) to create a fresh unused surface that separated the mouldable Blu-Tack®; from each flake. Thus, the artefacts never came into direct contact with the Blu-Tack®.

3.2 Reflected visible light microscopy (VLM)

A sample of 138 lithics were examined using reflected VLM for residues from Star Carr. Microscopic observations revealed deposits that were hypothesised to be resin, silicified plant remains, possibly phytoliths and wood tissue. However, since these residues did not contain structures which could be diagnostically assigned based on microscopic visual characteristics (see Croft et al., 2016), they were investigated with micro-Raman. VLM examination was used as a preliminary

analytical step to identify deposits on stone tools that were potential residues of human activity.

For the reflected VLM analysis, a low-power Leica MZ75 stereomicroscope at magnifications from 6.3-50x and a high-power Leica DM1750 M with objectives ranging from 5x to 100x, and an eyepiece magnification of 16x, were used. The locations of residues for investigation with micro-Raman were noted on printed photographs of each lithic and z-stacked micrographs of residues were taken with Leica Montage software.

3.3 Raman microspectroscopy (micro-Raman)

Micro-Raman was used to test the hypothesised identities of residue types and determine if the chemical signatures collected were consistent with resin and siliceous plant micro-remains. Raman spectroscopy is used to identify inorganic and organic molecular species of solid, liquid, or gas samples. A unique 'fingerprint' of a specific molecule is provided by IR and Raman spectra, based on the mass of the atoms, their geometric arrangement, and the types of chemical bonds present in the molecule (Larkin, 2011). Like FTIR, Raman spectroscopy is a type of vibrational spectroscopy and measures the interactions between laser photons and molecular bonds. The sample is irradiated with a visible or near-IR monochromatic laser, and the resulting scattered radiation is measured with a photo-spectrometer (Skoog et al., 2007). An unknown molecule can be identified because it exhibits a unique spectroscopic pattern of frequencies (Koenig, 2000) that can be recognised by comparison with spectral libraries and published literature, but can also be calculated based on the quantum-chemical approaches such as density functional theory (Johnson and Florián, 1995).

There are three major advantages of using micro-Raman to investigate archaeological artefacts. Firstly, this technique allows chemical characterisation of materials with a high degree of molecular specificity. Secondly, it is minimally invasive to the residue using a laser spot size of nominally 1 μm and is usually considered a non-destructive technique. That being said, under high laser power conditions damage can occur for specific residues. Thirdly, the residue can be analysed in situ on the non-uniform surfaces of the stone tool with generally no sample preparation required. Further, the surface morphology, in particular roughness is found to affect the measured Raman signal (Beard et al., 2011).

Micro-Raman has been used for various investigations in archaeology, from the analysis of bitumen residues on stone tools (Monnier et al., 2013), to anthropogenic pyrite traces on flint fire-strikers (Lombardo et al., 2016), and pigments on Roman statues (Cosano et al., 2017). At Star Carr, micro-Raman was recently used to

identify naturally-formed authigenic pyrite microcrystals on the surfaces of an engraved Mesolithic shale pendant (Milner et al., 2016).

A HORIBA Jobin Yvon Xplora confocal Raman microscope with LabSpec (version 6) and IGOR Pro software for peak analysis were used to collect and evaluate spectra. Long working distance microscope objectives were used to prevent an unintended direct contact between lens and object during sample analysis. A green Nd:YAG diode laser at 532 nm wavelength was used and the beam was focused through 10x and 50x microscope objectives on the sample at small spots of 1-5 μm in diameter. Maximum laser power used was 20 mW. Acquisition time was 20-30 seconds, number of accumulations (repetitions) was 10-20, and grating was 2400 grooves/mm. Polynomial baseline corrections were applied to all Raman spectra to remove fluorescence background using the software LabSpec6 and CrystalSleuth. This corrected data was plotted using Origin 2016 software, then labelled using Adobe Illustrator CS6. Once Raman spectra were collected, the band positions were compared to spectral database reference libraries, as well as published literature, to identify the material. The bulk flint of one of the artefacts was tested and compared to the spectra collected from the residues. The bulk flint was characterised as mainly α-quartz (SiO_2), with evidence for inclusion of moganite (SiO_2), a polymorph of α-quartz with a different crystal structure.

4. Results

4.1 Resin?

Just over half (54%) of all artefacts examined (n=138) contained red-orange deposits, from contexts in the waterlogged and dryland areas of Star Carr. It is plausible that hafting and/or resinous residues survive on Mesolithic tools, and particularly in the burial conditions at Star Carr, since birch bark tar was previously identified at the site by GC-MS by Aveling and Heron (1998), and conifer resin on flint was one of the best preserved residues found after experimental burial at Star Carr (Croft et al., 2016).

4.1.1 Microscopic description

At least four main morphologies or types of red-orange deposits were observed on flint stone tools: bounded amorphous, diffuse amorphous, tideline, and ‘casts’ of plant tissues. The bounded amorphous red-orange deposits had clear boundaries and usually exhibited a liquid pool or droplet-like appearance (Fig. 2). However, some bounded amorphous deposits were cracked and plate-like, sometimes with

microlamination visible. The diffuse amorphous deposits appeared like localised areas of misted or splattered coating. This diffuse red-orange deposits were always found in combination with the more discrete bounded amorphous deposits (see example on dorsal proximal flat surface of blade 93327, Fig. 2). Sometimes the diffuse deposits were seen emanating outwards from the bounded deposits.

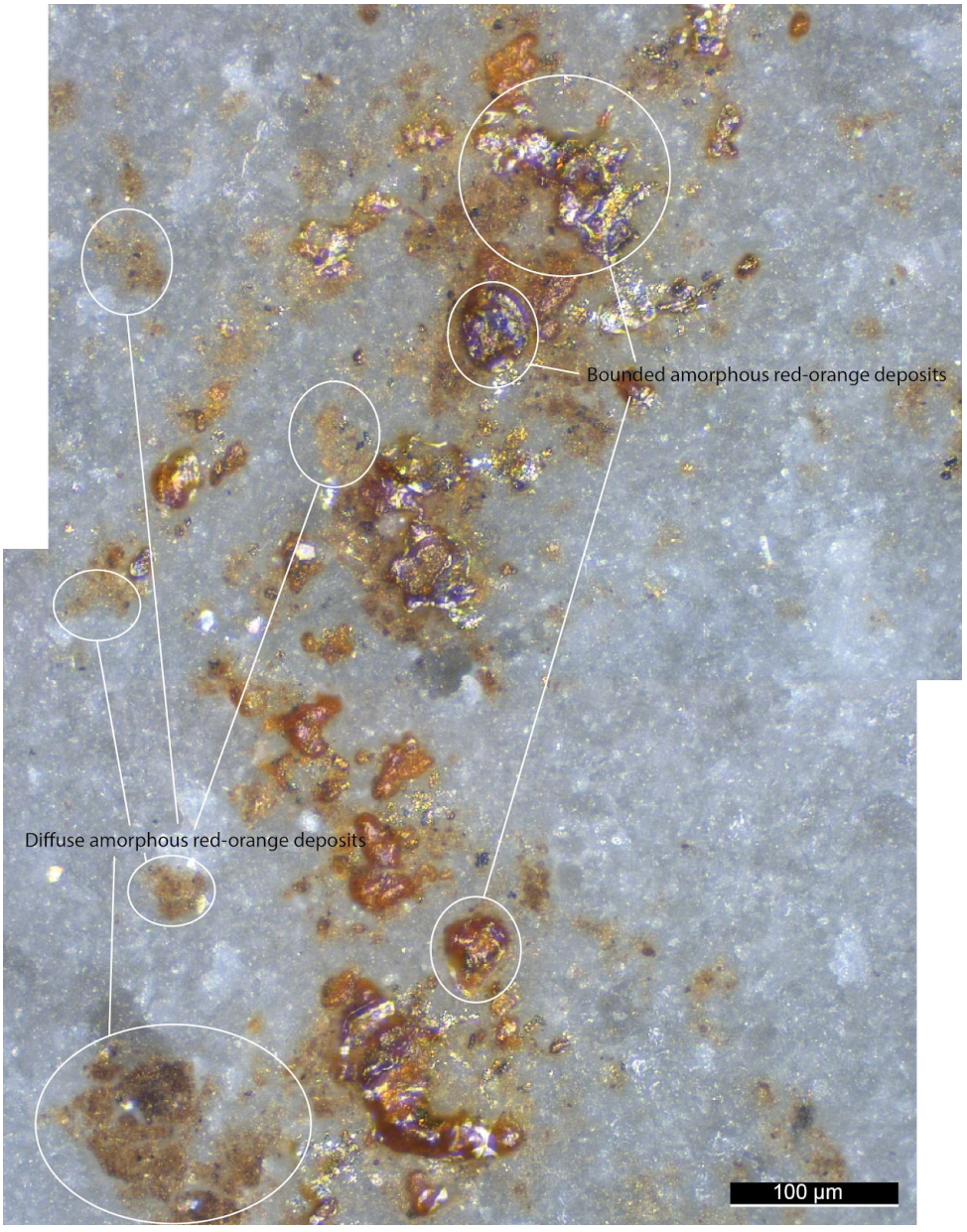

Fig. 2. Diffuse amorphous red-orange deposits and bounded amorphous deposits with a fluid, droplet-like appearance, found together on the dorsal proximal flat surface of blade 93327.

The red-orange tideline deposit appeared as a slightly wavy line (Fig. 3). It is possible that these represent the edge or extent where dissolved iron minerals precipitated out of the groundwater. This might be similar to the process that occurs when a salt oasis or lake undergoes drying, leaving salt evaporites in place where the margins were. The fourth morphology observed was red-orange plant tissue

casts that had visible cell walls (Fig. 3). The cell walls were raised and sometimes partially infilled, not an impression in a viscous resinous material.

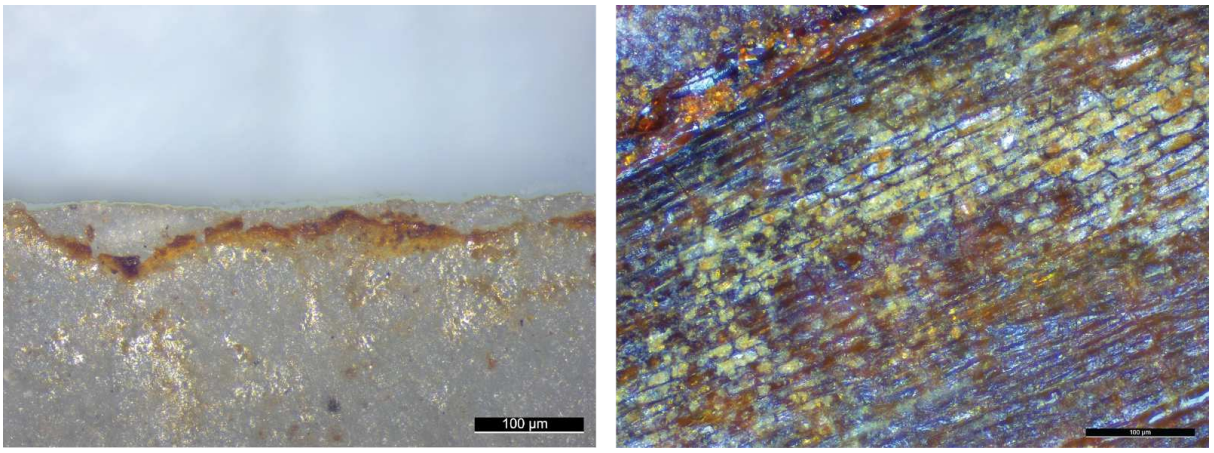

Fig. 3. Left: red-orange tideline deposit in association with diffuse deposits on dorsal left mid-edge of microlith 113623. Right: Micrograph of red-orange deposit which appears to have infilled the cell walls of plant tissues, creating a cast (possibly epidermal cells of reed leaves such as *Typha* sp.) on blade 108228. Deposit located on dorsal mid-centre surface of blade. These deposits were not confined to a single edge or the proximal area of the blade, as might be expected of a haft, but rather were present all over the tool.

4.1.2 Micro-Raman analysis

Red-orange deposits on three flint artefacts (94362, 94445, and 95828) were investigated using micro-Raman, and one of the spectra collected from blade 94445 is presented here. Shiny red-orange deposits were macroscopically visible on blade 94445. On the dorsal side these deposits appeared as lines, several centimetres long and about 3 mm wide. Microscopically, all four morphologies of red-orange deposits (bounded amorphous, diffuse amorphous, tideline, and plant tissue casts) were found. Specific points on the residue were investigated with the Raman laser.

Whilst manipulating blade 94445 on the microscope stage mount, three small pieces of the red-orange residue deposits were unintentionally dislodged from the flint. These residue fragments were collected from the clean parafilm surface with non-powdered gloves and placed in a sterile glass vial for storage and transport. For micro-Raman spectroscopy, the fragments were placed on a potassium bromide KBr support, on top of a microscope slide (Fig. 4). The KBr surface was used to minimize background Raman scattering. The flattest fragment (mid size piece) was investigated, with the red side facing the laser.

Fig. 4. Left: Blade 94445 with red-orange plant tissue cast deposits on the dorsal surface, sampled location circled.

The Raman spectra obtained from the red-orange deposits are consistent with iron (III) oxide (known as haematite). Iron (III) oxide (Fe_2O_3) has several known polymorphs. Polymorphs share the same chemical formula, but have different crystal structures due to different arrangements of the molecules, resulting in different vibrational properties. The four polymorphs of iron (III) oxide are: α-Fe_2O_3 (hexagonal corundum structure), γ-Fe_2O_3 (cubic spinel structure), β-Fe_2O_3 (cubic bixbyite structure), and ε-Fe_2O_3 (orthorhombic structure) (Zboril et al., 2003, 2002). The Raman bands (wavenumbers, cm^{-1}) shown in Fig. 5 at 220, 288, 405, ~597, and 1308 cm^{-1} match well with the reference values for α-Fe_2O_3 (Beattie and Gilson, 1970; Bonneau et al., 2017; Burgio and Clark, 2001; Courtin-Nomade et al., 2009; Das and Hendry, 2011; de Faria et al., 1997; de Faria and Lopes, 2007; de Tercero et al., 2014; Edwards et al., 2001; Froment et al., 2008; Legodi and de Waal, 2007; Mortimore et al., 2004; Oh et al., 1998; Ohtsuka et al., 1986).

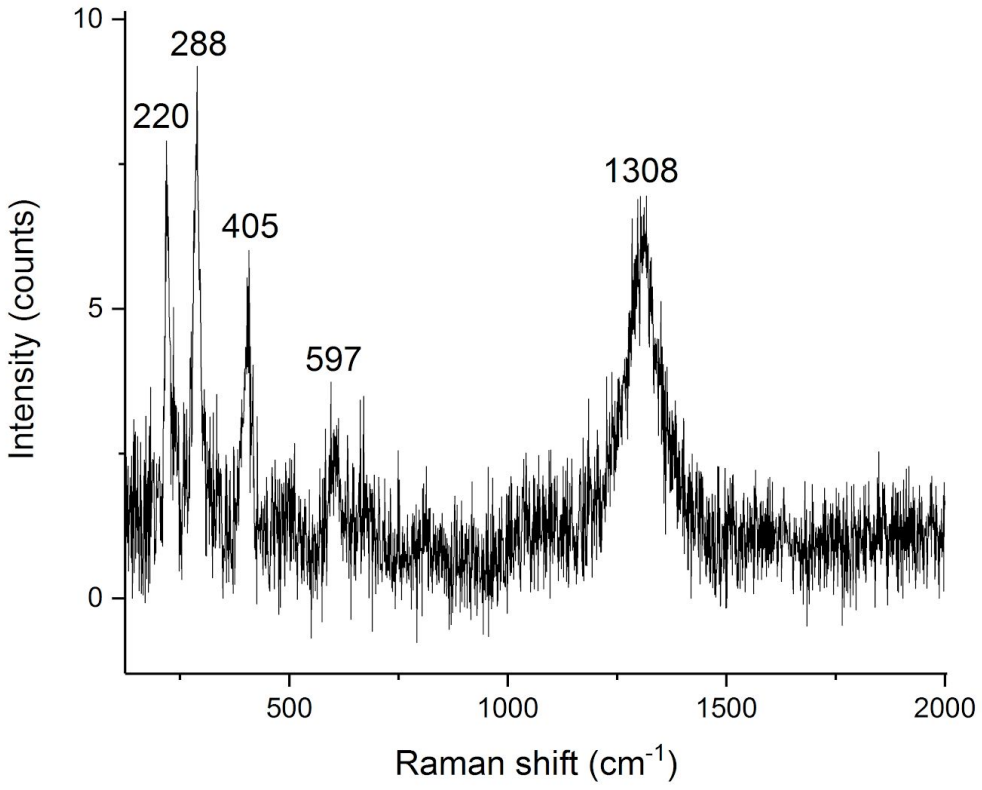

Fig. 5. A Raman spectrum collected from a red-orange plant tissue cast deposit on blade 94445, illustrating the deposit is iron (III) oxide.

4.2 Siliceous phytoliths or wood remains?

Microscopic crystalline structures were frequently encountered during VLM analysis, sometimes within a shiny deposit on the tool, sometimes isolated on the tool surface. These colourless crystals were found on 44 of 138 (32%) of the artefacts analysed from Star Carr. On initial discovery, it was thought that the colourless crystals were biogenic silica phytoliths from plant material or remnants of woody tissue. Lending support to this hypothesis was the fact that the microscopic structures occurred in the same recurring shapes, and were often located within what appeared to be usewear polish. Examples of polish with phytoliths embedded due to plant working activities have been reported previously, such as for Danish Neolithic stone tools (Anderson, 1980), and Australian Pleistocene grinding stones (Fullagar and Field, 1997). Thus, it seemed reasonable to expect plant working residues and polishes, perhaps from the processing of reeds or grasses for mats, baskets, roofing, clothing, and other items, on flint tools from Star Carr.

All but one of the tools containing clear crystals were recovered from acidic peats in the wetland part of Star Carr. Given this trend, it is suggested that there is likely a relationship between the presence of acidic organic sediment and the formation of colourless crystals on stone tools.

4.2.1 Microscopic description

Crystals were always clear and colourless. Lath, fine needle, rhombus, rosette (two types), twinned swallowtail, and fibrous sheet formations were observed, occasionally with a combination of these shapes occurring together on an artefact (see example, Fig. 6). The lath crystals were narrow, thin, elongate, blade-like shapes, and often had tapered ends.

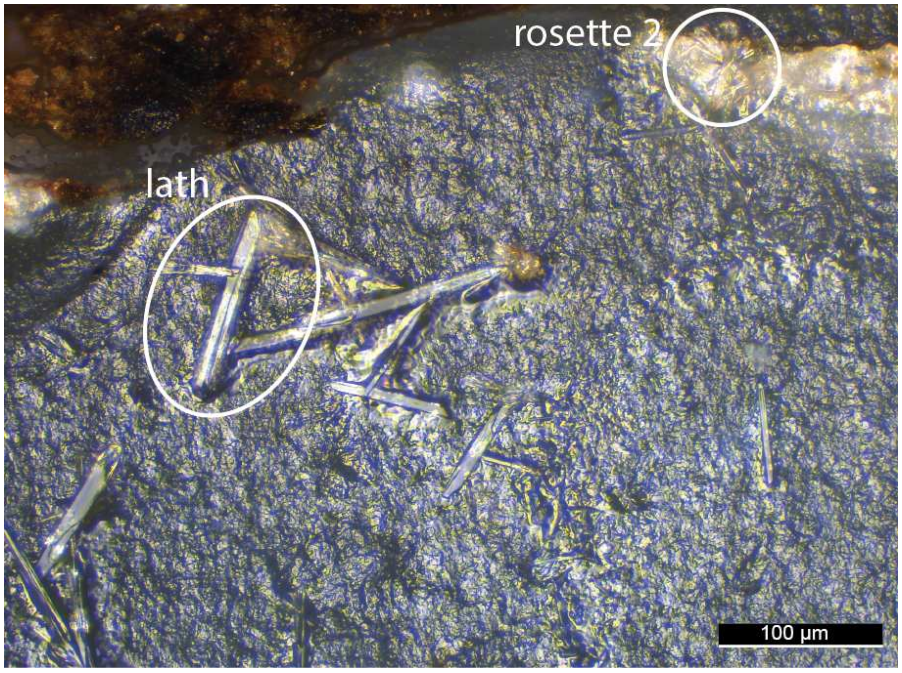

Fig. 6. Lath and rosette crystals found together on ventral left mid edge of blade fragment 108229.

Fine needle was an acicular crystal habit and can also be described as narrow, thin, and elongate, however with a smaller width than the lath shapes (Fig. 7). Rhombus-like crystals were diamond shaped with edges of equal length and opposite sides parallel (Fig. 7).

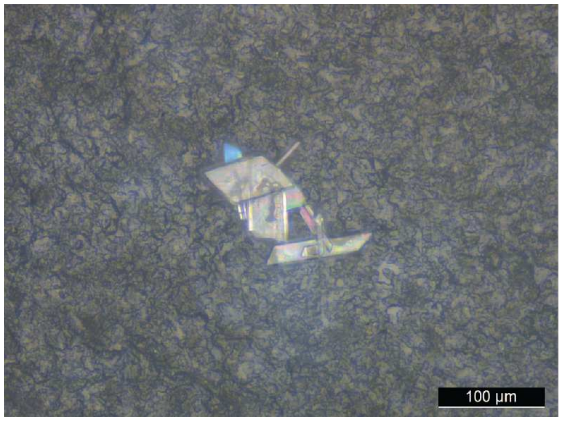

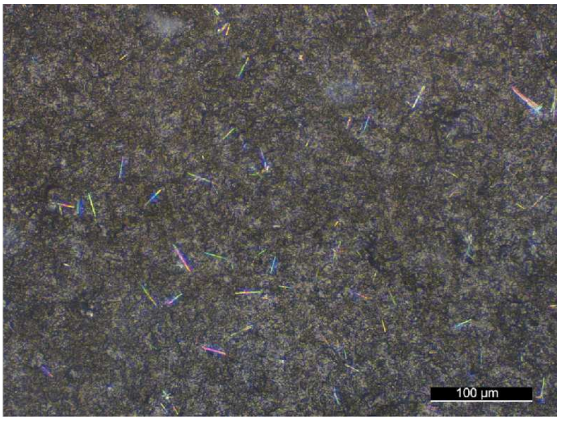

Fig. 7. Left: Rhombus and lath crystals on blade 99496, ventral proximal end, ~250 µm inwards from the tool edge. Right: Example of fine needle shaped crystals on blade 98086, located on left distal edge near some cortex on the flint.

The rosette 1 crystal habit was made up of groups of fine linear crystals radiating from a central point. In addition to being identified on stone tool surfaces, the rosette 1 habit was also observed in sediment samples from Star Carr. A second rosette shape was found during reflected VLM analysis. Rosette 2 was composed of random blocky lath crystals appearing as fibrous offshoots emanating approximately from a centre (Fig. 6, above).

Twinned microstructures were another type of colourless crystal encountered. On initial inspection, these twinned microstructures appeared somewhat similar to rondel shaped grass phytoliths (Piperno, 2006). However, closer inspection revealed that these structures more closely resembled crystals of mineralogical origin. The twinned crystals observed were about 40-90 µm and appear to be mirrored or double swallowtail twins, since both ends of each crystal exhibit the swallowtail (see gypsum crystals, Jafarzadeh and Burnham, 1992, p. 418 Fig. 1e) (Fig. 8).

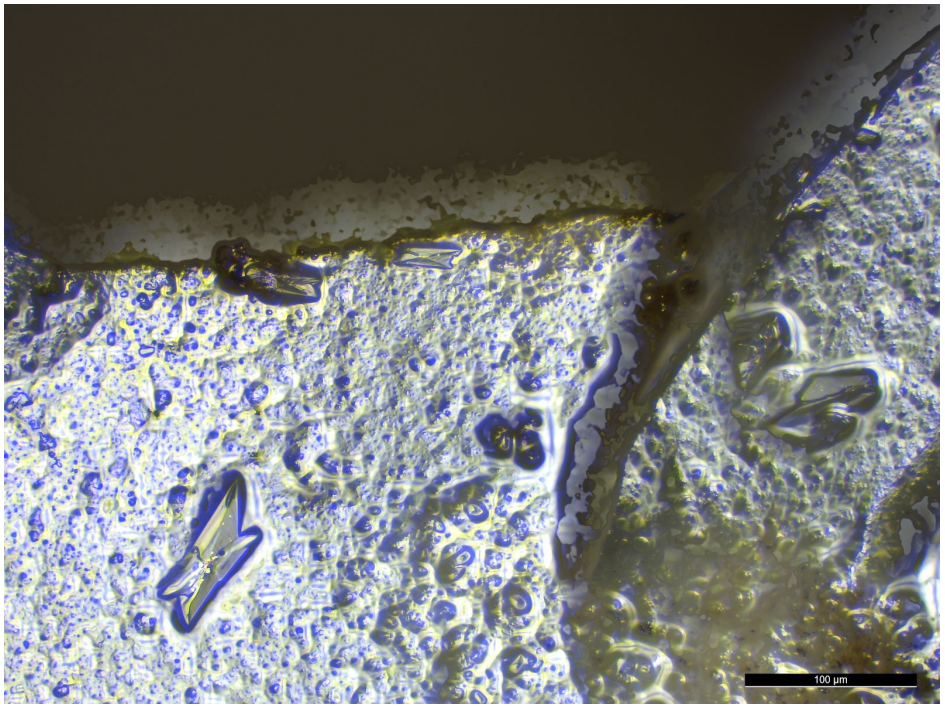

Fig. 8. Twinned crystals surrounded by a shiny deposit on the ventral distal right edge of flake tool 108237.

The last shape of colourless crystal formations exhibited on tools were fibrous sheet crystals. These ‘sheets’ were elongate and tightly packed parallel crystals. When observed in situ on stone tools, these crystals appear similar in appearance to articulated vascular tissue, such as wood tracheids and vessel elements but can be discounted based on a lack of pores (Fig. 9). Microscopic gypsum is known to form

flattened and sheet-like crystals (Önalgil et al., 2015/2, p. 120, Fig. 6b), and masses of fibrous gypsum occurring in parallel alignment have been found in natural and experimental soils by Jafarzadeh and Burnham (1992, p. 414 plate 9).

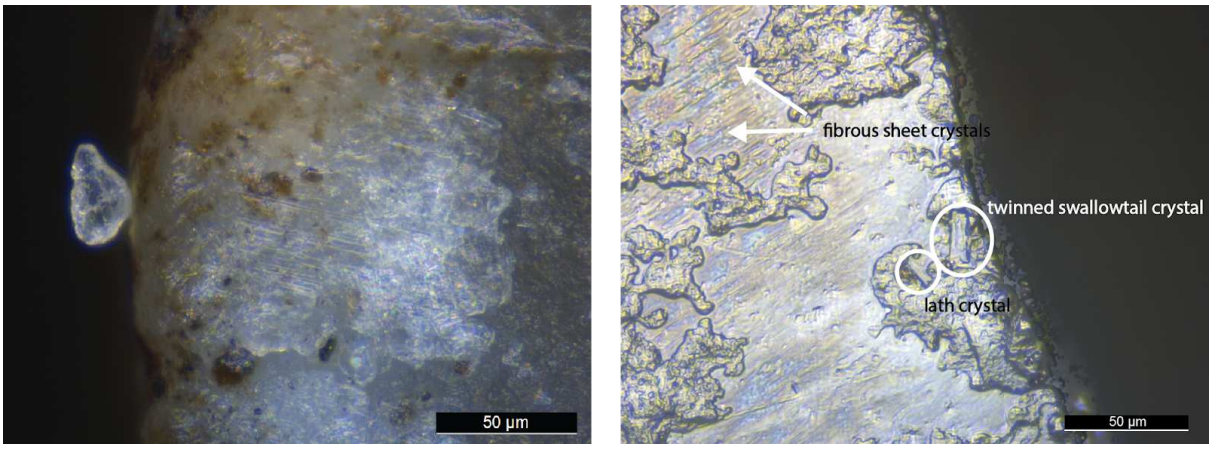

Fig. 9. Left: Originally interpreted as possible tracheids or vessel elements embedded in polish, these are likely actually gypsum in sheet formation. Residue found on core axe tool 99454, dorsal surface, along the right and left edges of the proximal end point. Right: Fibrous sheet crystals arranged in parallel alignment within shiny deposits on flake tool 108237, dorsal left mid-edge. Lath and twinned swallowtail crystals also visible in right image.

4.2.2 Micro-Raman analysis

Twinned swallowtail shaped crystals were found embedded in a shiny deposit on flake tool 99756, located on the ventral distal tip (Fig. 10). A location on one of these crystals was investigated with micro-Raman (spectrum illustrated in Fig. 11).

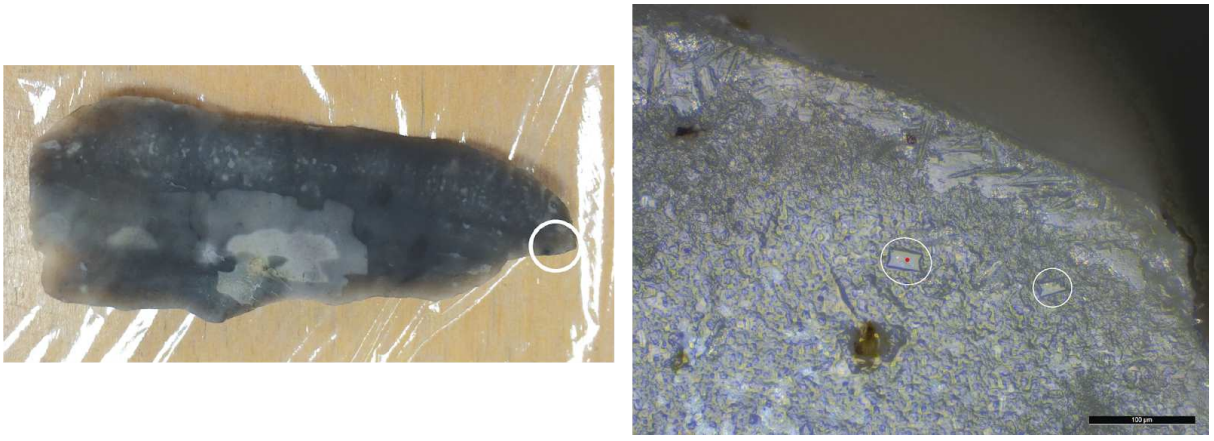

Fig. 10. Left: Flake tool 99756. Circled area shows where twinned swallowtail crystals embedded in a shiny were found, on the ventral distal tip, slightly right. Right: Twinned swallowtail crystals in a deposit on flake tool 99756, located on the ventral tip, slightly right. The red dot shows the location investigated with the Raman laser, corresponding to the spectrum below.

The Raman spectra collected from the twinned swallowtail crystals on flake tool 99756 show bands of correspondence with published reference spectra for gypsum

(calcium sulfate dihydrate, $CaSO_4 \cdot 2H_2O$) (Burgio and Clark, 2001; Buzgar et al., 2009; Colomban, 2011; Krishnamurthy and Soots, 1971; Li et al., 2009; Prieto-Taboada et al., 2014; Sarma et al., 1998; White, 2009). The most intense peak in gypsum is found at 1006 to 1010 cm^{-1}, attributed to the v_1 symmetric stretch vibration mode of SO_4 tetrahedra (Buzgar et al., 2009), which was present in the spectra from the twinned swallowtail crystals. The twinned swallowtail crystals showed a less intense bands at 206 cm^{-1}, which is assigned to translational lattice mode (H_2O), rotational lattice mode (SO_4) (Krishnamurthy and Soots, 1971; Sarma et al., 1998), and also a band at 494 cm^{-1}, which is assigned to v_2 symmetric bending of SO_4 (Prieto-Taboada et al., 2014). The band at 463 cm^{-1} is not reported in the literature for gypsum, and likely arises from the flint substrate, not the residue. This band matches with a major band of α-quartz and represents symmetric stretching-bending SiO_2 (A_1 mode) (Götze et al., 1998; Kingma and Hemley, 1994). The band at 1565 cm^{-1} is most likely caused by organics left by traces of sediment and is related to sp^2 carbon bonds (Cuesta et al., 1994; Dresselhaus et al., 2010; Tuinstra and Koenig, 1970).

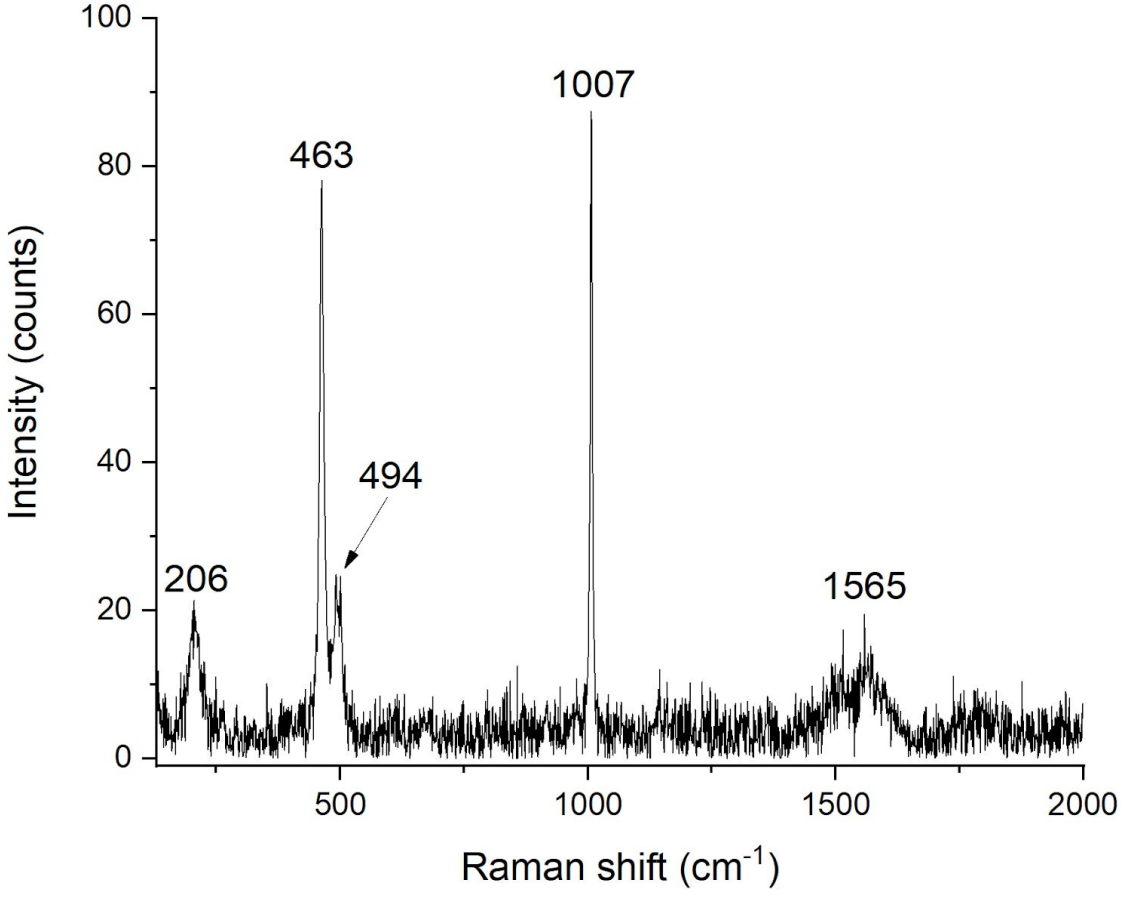

Fig. 11. Micro-Raman spectrum collected from a twinned swallowtail microcrystal on flake tool 99756.

5. Discussion

5.1 Introduction

Natural chemical processes occurring in the sediments at Star Carr are likely responsible for the presence of iron oxide, and gypsum minerals on lithic surfaces. However, our findings have wider implications for the practice of archaeological residue analysis. Some of the pedogenic residues observed here are likely also present at other archaeological sites and could complicate the interpretation of anthropogenic residues. For instance, micro-Raman investigations by Bordes et al. (2017) found natural iron oxides on stone tools originating from cave sediments at Liang Bua, Indonesia – a context completely different than Star Carr both geographically and sedimentologically. Gypsum and pyrite framboids have been found on other Mesolithic bone samples within or below waterlogged peat deposits from other sites the Vale of Pickering, including Flixton I and Flixton II (Turner-Walker, 1993). At another site site in Norfolk, UK, Turner-Walker (1998) confirmed the presence of gypsum and iron pyrite on Pleistocene elephant bones from the West Runton Freshwater Bed by X-ray diffraction (XRD). We thus suggest that gypsum and pyrite may be common contaminants on lithics and other artefacts from wetland anoxic sites, such as peats and bogs.

5.2 How did iron (III) oxide deposits form on lithics?

Iron oxides are known to be ubiquitous in soils and are the fourth most abundant mineral in the lithosphere by mass (Schwertmann and Cornell, 2000). At Star Carr, geochemical analysis (inductively coupled plasma atomic emission spectroscopy, ICP-AES) by Boreham et al. (2011a, 2011b) showed a pattern of elevated iron at the top and base of most borehole sequences taken across the site. Additionally, Boreham et al. (2011a, 2011b) found that high concentrations of iron were often associated with elevated sulfur concentrations. High (2014) hypothesised that the correlation between high levels of iron and sulfur was due to the presence of pyrite (FeS_2) in the underlying Speeton and Kimmeridge clays (Dypvik, 1984). Thus, chemical and biological oxidation of pyrite and the release of iron into sediments may be a main source contributing to the formation of iron (III) oxides on artefacts.

5.3 How did gypsum form on lithics?

It is most probable that gypsum crystals formed on tools as evaporite minerals derived from the sediments at Star Carr. Gypsum readily dissolves in water and sediment solutions, and crystals of gypsum precipitate as the water evaporates (FitzPatrick, 1984; Jafarzadeh and Burnham, 1992), in this case, onto tool surfaces.

Gypsum is also known to form as a by-product of pyrite oxidation in acid sulfate soils exposed to drainage (Miedema et al., 1974; Ritsema and Groenenberg, 1993). Pyrite oxidation also yields sulfuric acid (H_2SO_4). When sulfuric acid reacts with any Ca-bearing minerals, such as the calcium carbonate ($CaCO_3$) present in the lake marl sediments at Star Carr, or the chalk cortex of the flint tools themselves, precipitation of gypsum occurs. Boreham et al. (2011a a) suggests that the calcium carbonate from the lake marl reacts with acid sulfate to form selenite (gypsum) in Star Carr sediments.

6. Conclusion

It is proposed that a fourth major issue exists in the field of lithic residue analysis: residues may be identified incorrectly based on insufficient information. This is a substantial problem because a number of archaeological interpretations of ancient human and neanderthal behaviour, as well as inferences about cognitive abilities, have hinged on microscopic results. The findings of Monnier et al. (2012) and Croft et al. (2016) have already shown that many residue types are actually unidentifiable with reflected VLM because no specifically diagnostic structures are present. Thus, previously published claims of the discovery of particular lithic residues may need to be reexamined.

This study has shown that the visual microscopic strategy for identification of residues, when used as the only method of investigation, can be misleading. Many residues encountered on lithics from Star Carr might have been incorrectly interpreted as anthropogenic resin and siliceous plant remains on the basis of the microscopic analysis alone. However, the testing of the microscopic observations of residues by application of micro-Raman showed that:

- Red-orange deposits that appeared like resin were actually the alpha phase of iron (III) oxide (α-Fe_2O_3).
- Tiny clear crystal formations that appeared as silica plant phytoliths were actually gypsum (calcium sulfate dihydrate, $CaSO_4 \cdot 2H_2O$).
- Fibrous sheet formations which appeared like elongated articulated wood residues were actually gypsum.

The approach taken here – where the identity of each residue type was formulated as a hypothesis based on visual clues that served as a starting point for further chemical investigations – was successful. It was found that the results align with the chemical conditions at Star Carr, and the potential residue contribution of the burial

environment needs to be seriously considered in any residue analysis. Residue analysis is beginning to move past reliance on visual methods for the identification of ambiguous residues. For now, lithic residue analysis remains a time-intensive approach, requiring microscopic analysis and conservative interpretation, in conjunction with appropriate chemical characterisation techniques.

Acknowledgements

SC thanks the Social Sciences and Humanities Research Council of Canada for the fellowship grant that allowed this research to be carried out. The Star Carr project has received funding from the European Research Council (ERC) under the European Union's Seventh Framework Programme (FP7/2007-2013) under grant agreement No 283938; British Academy Grants SG-44333, SG-47081, and SG-50217; English Heritage/Historic England Grants 5536, 6064, 6793, 6796 and the radiocarbon dating of the site; Natural Environment Research Council Grant NE/I015191/1; The Vale of Pickering Research Trust; The Universities of Manchester, York, and Chester. We are grateful to the landowners of Star Carr, English Heritage/Historic England, and Natural England for granting permission to excavate. We also thank Inga Kerber for assistance with Raman data processing. We appreciate the valuable comments that anonymous reviewers provided.

References

Anderson, P.C., 1980. A Testimony of Prehistoric Tasks: Diagnostic Residues on Stone Tool Working Edges. World Archaeol. 12, 181–194.

Aveling, E.M., Heron, C., 1998. Identification of birch bark tar at the Mesolithic site of Star Carr. Anc. Biomol. 2, 69–80.

Bayliss, A., Taylor, B., Ramsey, C.B., Dunbar, E., M., K.B.B., Conneller, C., Elliot, B., Knight, B., Milner, N., in press. Dating the archaeology and environment of the Star Carr embayment, in: Milner, N., Conneller, C., Taylor, B. (Eds.), Star Carr Monograph. White Rose Press, York.

Beard, M.A., Ghita, O.R., Evans, K.E., 2011. Using Raman spectroscopy to monitor surface finish and roughness of components manufactured by selective laser sintering. J. Raman Spectrosc. 42, 744–748.

Beattie, I.R., Gilson, T.R., 1970. The single-crystal Raman spectra of nearly opaque materials. Iron (III) oxide and chromium (III) oxide. J. Chem. Soc. A 980–986.

Bleicher, N., Kelstrup, C., Olsen, J.V., Cappellini, E., 2015. Molecular evidence of use of hide glue in 4th millennium BC Europe. J. Archaeol. Sci. 63, 65–71.

Bonneau, A., Moyle, J., Dufourmentelle, K., Arsenault, D., Dagneau, C., Lamothe, M., 2017. A Pigment Characterization Approach to Selection of Dating Methods and Interpretation of Rock Art: The Case of the Mikinak Site, Lake Wapizagonke, Quebec, Canada. Archaeometry. https://doi.org/10.1111/arcm.12289

Bordes, L., Prinsloo, L.C., Fullagar, R., Sutikna, T., Hayes, E., Jatmiko, Wahyu Saptomo, E., Tocheri, M.W., Roberts, R.G., 2017. Viability of Raman microscopy to identify micro-residues related to tool-use and modern contaminants on prehistoric stone artefacts. J. Raman Spectrosc. 48, 1212–1221.
Boreham, S., Boreham, J., Rolfe, C.J., 2011b. Physical and Chemical Analyses of Sediments from around Star Carr as Indicators of Preservation. Journal of Wetland Archaeology 11, 20–35.
Boreham, S., Conneller, C., Milner, N., Taylor, B., Needham, A., Boreham, J., Rolfe, C.J., 2011a. Geochemical indicators of preservation status and site deterioration at Star Carr. J. Archaeol. Sci. 38, 2833–2857.
Burgio, L., Clark, R.J., 2001. Library of FT-Raman spectra of pigments, minerals, pigment media and varnishes, and supplement to existing library of Raman spectra of pigments with visible excitation. Spectrochim. Acta A Mol. Biomol. Spectrosc. 57, 1491–1521.
Buzgar, N., Buzatu, A., Sanislav, I.V., 2009. The Raman study on certain sulfates. Analele Ştiintifice ale Universităţii Al Cuza din Iaşi. Sect. 2, Geologie 55, 5–23.
Colomban, P., 2011. Pigment identification of a rare 18th century wallpaper from Buffon library. J. Raman Spectrosc. 42, 192–194.
Cosano, D., Mateos, L.D., Jiménez-Sanchidrián, C., Ruiz, J.R., 2017. Identification by Raman microspectroscopy of pigments in seated statues found in the Torreparedones Roman archaeological site (Baena, Spain). Microchem. J. 130, 191–197.
Courtin-Nomade, A., Grosbois, C., Marcus, M.A., Fakra, S.C., Beny, J.-M., Foster, A.L., 2009. The weathering of a sulfide orebody: speciation and fate of some potential contaminants. Canadian Mineralogist 47, 493–508.
Croft, S., Monnier, G., Radini, A., Little, A., Milner, N., 2016. Lithic residue survival and characterisation at Star Carr: a burial experiment. Internet Archaeology 42. https://doi.org/10.11141/ia.42.5
Cuesta, A., Dhamelincourt, P., Laureyns, J., Martínez-Alonso, A., Tascón, J.M.D., 1994. Raman microprobe studies on carbon materials. Carbon N. Y. 32, 1523–1532.
Das, S., Hendry, M.J., 2011. Application of Raman spectroscopy to identify iron minerals commonly found in mine wastes. Chem. Geol. 290, 101–108.
de Faria, D.L.A., Lopes, F.N., 2007. Heated goethite and natural hematite: Can Raman spectroscopy be used to differentiate them? Vib. Spectrosc. 45, 117–121.
de Faria, D.L.A., Venâncio Silva, S., de Oliveira, M.T., 1997. Raman microspectroscopy of some iron oxides and oxyhydroxides. J. Raman Spectrosc. 28, 873–878.
de Tercero, M.D., Röder, C., Fehrenbacher, U., Teipel, U., Türk, M., 2014. Continuous supercritical hydrothermal synthesis of iron oxide nanoparticle dispersions and their characterization. J. Nanopart. Res. 16, 1–27.
Dresselhaus, M.S., Jorio, A., Hofmann, M., Dresselhaus, G., Saito, R., 2010. Perspectives on carbon nanotubes and graphene Raman spectroscopy. Nano Lett. 10, 751–758.
Dypvik, H., 1984. Geochemical compositions and depositional conditions of Upper Jurassic and Lower Cretaceous Yorkshire clays, England. Geological Magazine 121, 489–504.
Edwards, H.G.M., Farwell, D.W., de Faria, D.L.A., Monteiro, A.M.F., Afonso, M.C., De Blasis, P., Eggers, S., 2001. Raman spectroscopic study of 3000-year-old human skeletal remains from a sambaqui, Santa Catarina, Brazil. J. Raman Spectrosc. 32, 17–22.
FitzPatrick, E.A., 1984. Micromorphology of Soils. Chapman and Hall, London.
Froment, F., Tournié, A., Colomban, P., 2008. Raman identification of natural red to yellow pigments: ochre and iron-containing ores. J. Raman Spectrosc. 39, 560–568.
Fullagar, R., Field, J., 1997. Pleistocene seed-grinding implements from the Australian arid zone. Antiquity 71, 300–307.
Götze, J., Nasdala, L., Kleeberg, R., Wenzel, M., 1998. Occurrence and distribution of “moganite” in agate/chalcedony: a combined micro-Raman, Rietveld, and

cathodoluminescence study. Contrib. Mineral. Petrol. 133, 96–105.
Grace, R., 1996. Use-wear analysis: the state of the art. Archaeometry 38, 209–229.
Haslam, M., 2006a. Archaeology of the instant? Action and narrative in microscopic archaeological residue analysis. Journal of Social Archaeology 6, 402–424.
Helwig, K., Monahan, V., Poulin, J., Andrews, T.D., 2014. Ancient projectile weapons from ice patches in northwestern Canada: identification of resin and compound resin-ochre hafting adhesives. Journal of Archaeological Science 41, 655–665.
High, K., 2014. Fading Star: Understanding Accelerated Decay at Star Carr. University of York.
Jafarzadeh, A.A., Burnham, C.P., 1992. Gypsum crystals in soils. Journal of Soil Science 43, 409–420.
Johnson, B.G., Florián, J., 1995. The prediction of Raman spectra by density functional theory. Preliminary findings. Chem. Phys. Lett. 247, 120–125.
Kingma, K.J., Hemley, R.J., 1994. Raman spectroscopic study of microcrystalline silica. American Mineralogist 79, 269–273.
Koenig, J.L., 2000. Infrared and Raman Spectroscopy of Polymers, Rapra Review Reports: Expert overviews covering the science and technology of rubber and plastics. Smithers Rapra Press, Belfast.
Krishnamurthy, N., Soots, V., 1971. Raman Spectrum of Gypsum. Canadian Journal of Physics 49, 885–896.
Langejans, G.H.J., 2009. Testing Residues: An Experimental Approach. University of Witwatersrand, Johannesburg.
Larkin, P., 2011. Infrared and Raman Spectroscopy; Principles and Spectral Interpretation. Elsevier.
Legodi, M.A., de Waal, D., 2007. The preparation of magnetite, goethite, hematite and maghemite of pigment quality from mill scale iron waste. Dyes Pigm. 74, 161–168.
Li, T., Xie, Y.-F., Yang, Y.-M., Wang, C.-S., Fang, X.-Y., Shi, J.-L., He, Q.-J., 2009. Pigment identification and decoration analysis of a 5th century Chinese lacquer painting screen: a micro-Raman and FTIR study. J. Raman Spectrosc. 40, 1911–1918.
Lombardo, T., Grolimund, D., Kienholz, A., Hubert, V., Wörle, M., 2016. The use of flint-stone fragments as “fire-strikers” during the Neolithic period: Complementary micro-analytical evidences. Microchem. J. 125, 254–259.
Luong, S., Hayes, E., Flannery, E., Sutikna, T., Tocheri, M.W., Wahyu Saptomo, E., Jatmiko, Roberts, R.G., 2017. Development and application of a comprehensive analytical workflow for the quantification of non-volatile low molecular weight lipids on archaeological stone tools. Anal. Methods. https://doi.org/10.1039/C7AY01304C
Miedema, R., Jongmans, A.G., Slager, S., 1974. Micromorphological observations on pyrite and its oxidation products in four Holocene alluvial soils in the Netherlands, in: Rutherford, G.K. (Ed.), Soil Microscopy: Proceedings of the Fourth International Working-Meeting on Soil Micromorphology. Department of Geography, Queen’s University, Kingston, pp. 772–794.
Milner, N., Bamforth, M., Beale, G., Carty, J.C., Chatzipanagis, K., Croft, S., Conneller, C., Elliott, B., Fitton, L.C., Knight, B., Kroger, R., Little, A., Needham, A., Robson, H.K., Rowley, C.C.A., Taylor, B., 2016. A Unique Engraved Shale Pendant from the Site of Star Carr: the oldest Mesolithic art in Britain. Internet Archaeology 40. https://doi.org/10.11141/ia.40.8
Monnier, G.F., Hauck, T.C., Feinberg, J.M., Luo, B., Le Tensorer, J.-M., Sakhel, H. al, 2013. A multi-analytical methodology of lithic residue analysis applied to Paleolithic tools from Hummal, Syria. Journal of Archaeological Science 40, 3722–3739.
Monnier, G.F., Ladwig, J.L., Porter, S.T., 2012. Swept under the rug: the problem of unacknowledged ambiguity in lithic residue identification. J. Archaeol. Sci. 39,

3284–3300.
Monnier, G., Frahm, E., Luo, B., Missal, K., 2017a. Developing FTIR microspectroscopy for analysis of plant residues on stone tools. J. Archaeol. Sci. 78, 158–178.
Monnier, G., Frahm, E., Luo, B., Missal, K., 2017b. Developing FTIR Microspectroscopy for the Analysis of Animal-Tissue Residues on Stone Tools. J Archaeol Method Theory 1–44.
Mortimore, J.L., Marshall, L.-J.R., Almond, M.J., Hollins, P., Matthews, W., 2004. Analysis of red and yellow ochre samples from Clearwell Caves and Çatalhöyük by vibrational spectroscopy and other techniques. Spectrochimica Acta Part A: Molecular and Biomolecular Spectroscopy 60, 1179–1188.
Oh, S.J., Cook, D.C., Townsend, H.E., 1998. Characterization of iron oxides commonly formed as corrosion products on steel. Hyperfine Interact.
Ohtsuka, T., Kubo, K., Sato, N., 1986. Raman spectroscopy of thin corrosion films on iron at 100 to 150 C in air. Corrosion 42, 476–481.
Önalgil, N., Kadir, S., Külah, T., Eren, M., Gürel, A., 2015/2. Mineralogy, geochemistry and genesis of the modern sediments of Seyfe Lake, Kırşehir, central Anatolia, Turkey. J. Afr. Earth. Sci. 102, 116–130.
Pedergnana, A., Blasco, R., 2016. Characterising the exploitation of avian resources: An experimental combination of lithic use-wear, residue and taphonomic analyses. Quat. Int. 421, 255–269.
Piperno, D.R., 2006. Phytoliths: A Comprehensive Guide for Archaeologists and Paleoecologists. Altamira, Lanham.
Prieto-Taboada, N., Gómez-Laserna, O., Martínez-Arkarazo, I., Olazabal, M.Á., Madariaga, J.M., 2014. Raman Spectra of the Different Phases in the CaSO4–H2O System. Anal. Chem. 86, 10131–10137.
Ritsema, C.J., Groenenberg, J.E., 1993. Pyrite Oxidation, Carbonate Weathering, and Gypsum Formation in a Drained Potential Acid Sulfate Soil. Soil Science Society of America Journal 57, 968–976.
Sarma, L.P., Prasad, P.S.R., Ravikumar, N., 1998. Raman spectroscopic study of phase transitions in natural gypsum. J. Raman Spectrosc. 29, 851–856.
Schwertmann, U., Cornell, R.M., 2000. Iron Oxides in the Laboratory: Preparation and Characterization, 2nd ed. Wiley-VCH, Weinheim.
Skoog, D.A., James Holler, F., Crouch, S.R., 2007. Principles of Instrumental Analysis. Thomson Brooks/Cole.
Tuinstra, F., Koenig, J.L., 1970. Raman Spectrum of Graphite. J. Chem. Phys. 53, 1126–1130.
Turner-Walker, G., 1998. The West Runton fossil elephant: A pre-conservation evaluation of its condition, chemistry and burial environment. The conservator 22, 26–35.
Turner-Walker, G.H., 1993. The characterisation of fossil bone (Doctoral). Durham University.
White, S.N., 2009. Laser Raman spectroscopy as a technique for identification of seafloor hydrothermal and cold seep minerals. Chem. Geol. 259, 240–252.
Zboril, R., Mashlan, D., Petridis, D., Krausova, D., Pikal, P., 2002. Role of intermediates in the process of red ferric pigment manufacture from FeSO4 · 7H2O, in: Cook, D.C., Hoy, G.R. (Eds.), Industrial Applications of the Mössbauer Effect. Presented at the ISIAME 2000, Springer, Dordrecht, pp. 437–445.
Zboril, R., Mashlan, M., Machala, L., Bezdicka, P., 2003. Iron (III) oxides formed during thermal conversion of rhombohedral iron (III) sulfate, in: Mashlan, M., Miglierini, M., Schaaf, P. (Eds.), Material Research in Atomic Scale by Mössbauer Spectroscopy, NATO Science Series. Presented at the NATO Advanced Research Workshop on Material Research in Atomic Scale by Mössbauer Spectroscopy, Springer, Dordrecht,

pp. 21–30.